

AperTO - Archivio Istituzionale Open Access dell'Università di Torino

Elastic and Vibrational Properties of alpha- and beta-PbO

This is the author's manuscript

Original Citation:

Availability:

This version is available <http://hdl.handle.net/2318/128896> since 2016-08-07T18:28:34Z

Published version:

DOI:10.1021/jp3036988

Terms of use:

Open Access

Anyone can freely access the full text of works made available as "Open Access". Works made available under a Creative Commons license can be used according to the terms and conditions of said license. Use of all other works requires consent of the right holder (author or publisher) if not exempted from copyright protection by the applicable law.

(Article begins on next page)

This is the author's final version of the contribution published as:

P. Canepa; P. Ugliengo; M. Alfredsson. Elastic and Vibrational Properties of alpha- and beta-PbO. JOURNAL OF PHYSICAL CHEMISTRY. C, NANOMATERIALS AND INTERFACES. 116 pp: 21514-21522.
DOI: 10.1021/jp3036988

The publisher's version is available at:

<http://pubs.acs.org/doi/abs/10.1021/jp3036988>

When citing, please refer to the published version.

Link to this full text:

<http://hdl.handle.net/2318/128896>

Elastic and vibrational properties of α and β -PbO.

P. Canepa,^{*,†,‡} P. Ugliengo,[¶] and M. Alfredsson[†]

School of Physical Sciences, Ingram building, University of Kent, Canterbury CT2 7NH, United Kingdom, Department of Physics, Wake Forest University, 1834 Wake Forest Road, Winston-Salem, NC 27109, USA, and Dipartimento di Chimica, University of Torino, Via Pietro Giuria 7, Turin, 10125, Italy

E-mail: canepap@wfu.edu

KEYWORDS: Elastic constants, Phonons, Bulk moduli, EFG, DFT, DFT-D2, Layered materials

*To whom correspondence should be addressed

[†]School of Physical Sciences, Ingram building, University of Kent, Canterbury CT2 7NH, United Kingdom

[‡]Department of Physics, Wake Forest University, 1834 Wake Forest Road, Winston-Salem, NC 27109, USA

[¶]Dipartimento di Chimica, University of Torino, Via Pietro Giuria 7, Turin, 10125, Italy

Abstract

The structure, electronic and dynamic properties of the two layered α (litharge) and β (massicot) phases of PbO have been studied by density functional methods. The role of London dispersion interactions as leading component of the total interaction energy between layers has been addressed by using the Grimme's approach, in which new parameters for Pb and O atoms have been developed. Both gradient corrected and hybrid functionals have been adopted using Gaussian-type basis sets of polarized triple zeta quality for O atoms and small core pseudo-potential for the Pb atoms. Basis set superposition error (BSSE) has been accounted for by the Boys-Bernardi correction to compute the interlayer separation. Cross check with calculations adopting plane waves that are BSSE free have also been performed for both structures and vibrational frequencies. With the new set of proposed Grimme's type parameters structures and dynamical parameters for both PbO phases are in good agreement with experimental data.

1 Introduction

Lead monoxide (PbO) is largely employed for several industrial and technological applications such as electronic devices,¹⁻³ in special ceramic-glasses,^{4,5} for X-ray cathodes, for pigments,^{6,7} in rubber vulcanization^{8,9} and in the automotive sector as an essential component for batteries.^{10,11} PbO is largely found in two polymorphs: a tetragonal $P4/nmm$ phase (α -PbO or litharge) and an orthorhombic phase $Pbcm$ (β -PbO or massicot).

In α -PbO the Pb^{2+} ions are **pyramidally** coordinated by oxygen atoms (see Figure 1a) packed in a special layered-arrangement that resembles a distorted CsCl structure. This distortion is principally caused by free lone-pairs on the Pb^{2+} ions. The key element in the lone-pairs localizations is the hybridization of the $Pb(6s)$ and **$Pb(6p)$** orbitals with $O(2p)$ states as demonstrated by Watson *et al.*^{12,13} **Below 200 K the tetragonal α -PbO undergoes a phase transition to orthorhombic $Cmma$ as observed by Boher *et al.*;¹⁴ where the new a' and b' lattice parameters are redefined as $a' \approx a + b$, $b' \approx b - a$, where a and b are α -PbO lattice constants. The distorted α -phase can be regarded as intermediate PbO phase between α -and- β polymorphous. Very few studies are**

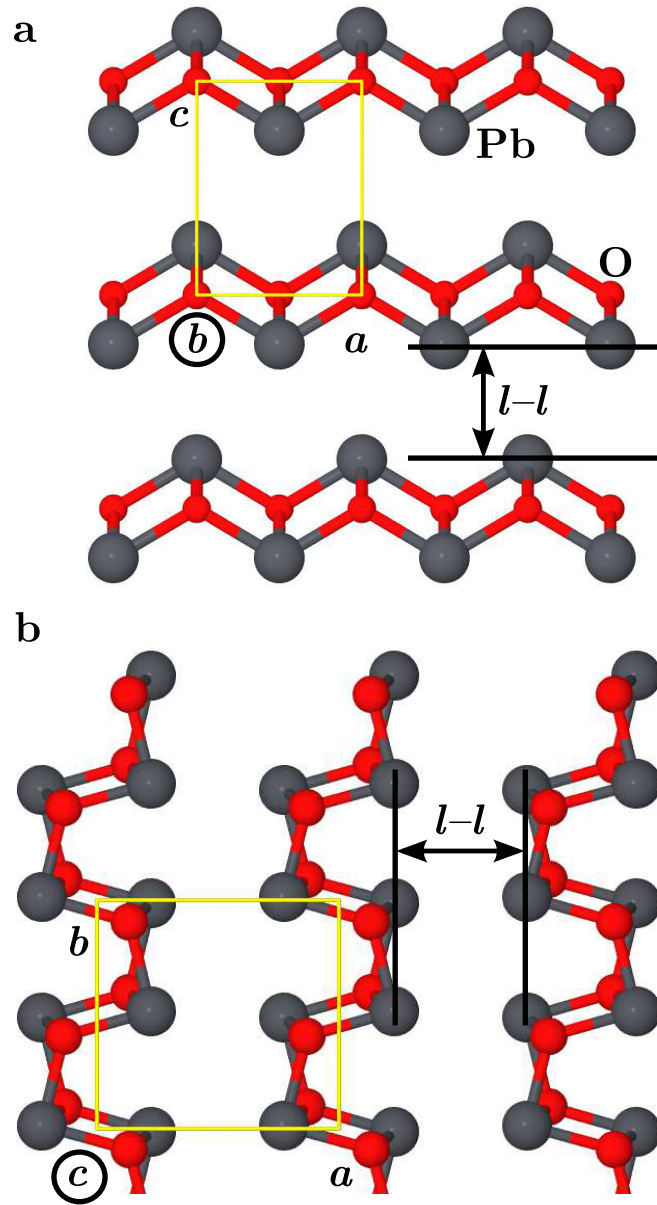


Figure 1: a) view along the $[010]$ direction of α -PbO ($P4/nmm$), and b) along the $[001]$ direction β -PbO ($Pbcm$). The inter-layer distance is highlighted as $l-l$.

available on β -PbO. This lead oxide polymorph is characterized by *zig-zag* chains of PbO units repeated along the b axis of the cell (see Figure 1b). As for litharge, Pb^{2+} ions are found **pyramidally**-coordinated by oxygen atoms although, forming squares parallel to the bc plane. The *zig-zag* chains are then stacked along the a axis forming a layered structure almost unique in nature. While previous theoretical works established the structure of both PbO polymorphs^{15–17} and the nature of the Pb lone-pairs,¹⁸ in this study we also address the role of dispersion interactions on the energetic, structure and dynamic properties of both phases.

As depicted in Figure 1 in both lead oxide polymorphs rippled two-dimensional planes are stacked in a peculiar layered arrangement. The layered nature of α and β -PbO suggest that dispersive interactions may play a key role in stabilizing these structures. Differently from classic post Hartree-Fock methods such as MP2 and CCSD(T), most common DFT-GGA and hybrid functionals are unable to deal with purely dispersive London forces originating from fluctuating dipole-dipole interactions. **Currently there are three main approaches to include dispersive forces in DFT:**¹⁹ *i)* the design of new functionals derived in a fully *ab initio* fashion as suggested by Lundqvist and coworkers;^{20–23} *ii)* a highly parametrized functionals of the M0X family as proposed by Thrular *et al.*;^{24,25} *iii)* an empirical correction to the standard DFT energy and gradient based on the empirical London formula as repurposed by Grimme and later improved by Tkatchenko *et al.*^{26–30} In this latter scheme, hereafter termed DFT-D2 (Grimme’s correction),^{26,27} an atom-atom empirical potential (of the form $f(R)C_6/R^6$) accounts for the dispersion on the DFT energy as follows:

$$E_{DFT+D2} = E_{DFT} + E_D \quad (1)$$

where E_D is the additive dispersion term.

2 Computational Details

Simulations presented here were performed with CRYSTAL09,^{31,32} using hybrid and plain functionals. We used three GGA-functionals: PBE,³³ PBEsol,³⁴ BLYP^{35,36} and two hybrid-GGA

functionals: B3LYP^{35–37} (20% HF exchange) and PBE0³⁸ (25% HF). Oxygen atoms were described with an all–electrons basis–set TPZ by Ahlrichs and co–workers (see Ref. 39). Pb core–electrons were described by an effective small core potential⁴⁰ along with a VDZ basis–set for the valence shells.⁴¹ We used a Monkhorst–Pack⁴² grid of 8x8x8 k –points **ensuring that the total energy is well converged**. The self–consistent–field (SCF) procedure is converged within 10^{-8} Hartree. The Coulomb and exchange series were truncated using stringent overlap criteria, *i.e.* 10^{-9} , 10^{-9} , 10^{-9} , 10^{-9} and 10^{-12} . Second–order elastic constants, $C_{i,j}$, were evaluated using the analytic total energy gradient and numerical second derivative with respect to the applied strain around the optimized equilibrium structure.⁴³ According to the symmetry of the second–order elastic strain tensor, the appropriate number of strains were applied; hence the internal coordinates were relaxed for each strain displacement. Bulk moduli were determined *via* the elastic constants (for tetragonal Voight averages: $\frac{1}{9}(2C_{11} + 2C_{12} + 4C_{13} + C_{33})$, and orthorhombic: $\frac{1}{9}((C_{11} + C_{22} + C_{33}) + 2(C_{12} + C_{13} + C_{23}))$). For these calculations we reduced the SCF tolerance to 10^{-9} Hartree, whereas those on the gradient and the rms displacement were 6×10^{-5} and 1.2×10^{-4} Hartree bohr⁻¹, respectively.⁴³ The dynamical matrix, at Γ point, was computed by finite differences: the atomic displacement was set to 3×10^{-3} Å, reducing the SCF tolerance to 10^{-11} Hartree.⁴⁴

Aware of the spurious basis set superposition error (BSSE) introduced by the LCAO treatment employed by CRYSTAL09, we performed some PBE–D2 and –DC2 calculations with a pseudopotential plane–wave (PP–PW) code *PWscf* (a Quantum ESPRESSO package),⁴⁵ which is BSSE free. We used ultra–soft pseudopotentials for Pb (**fully relativistic and with spin-orbit coupling correction**) and O, whereas remaining valence electrons were described with a plane–wave basis set with a cutoff of 950 eV, while the total energy was sampled over a 8x8x8 k –point grid. **Where not explicitly stated result were produced using CRYSTAL09.**

3 Dispersive forces

The empirical dispersion contribution E_D , of Eq. (1), is defined as:

$$E_D = -s_6 \sum_g \sum_{ij} \frac{C_6^{ij}}{R_{ij,g}^6} f_{dmp}(R_{ij,g}) \quad (2)$$

where the summations extend over all atomic pairs i, j and g lattice vectors. C_6^{ij} is the dispersion coefficient, and $s_6 = 0.75$ (see Ref. 27) is a functional dependent scaling factor. $R_{ij,g}$ is the inter-atomic distance between atoms i in the reference cell and j in the neighboring cells at distance $|g|$. All pairs farther than 25 Å were disregarded in the summations due to their negligible contribution. Double counting for small inter-atomic distances are avoided using the following damping function $f_{dmp}(R_{ij,g}) = 1/(1 + e^{-d(R_{ij,g}/R_{vdW}-1)})$ where R_{vdW} are the atomic van der Waals' radii, d is the damping function steepness ($d = 20$).²⁶ In Grimme's work R_{vdW} were set as the atomic van der Waals radii, which are 1.767 and 1.342 Å for Pb and O respectively. The definition of the C_6^{ij} coefficients of Eq. (3a)^{26,27} follows the well-known geometrical mean:

$$C_6^{ij} = \sqrt{C_6^i C_6^j}; \quad (3a)$$

$$C_6^i = 0.05 N I_p^i \alpha^i. \quad (3b)$$

In Eq. (3b), N , is the number of the shell electrons, and has values of 2, 10, 18, 36, 54 and 72 for atoms from rows 1–6 of the periodic table. The original Grimme's C_6^i parameters were derived from the atomic polarizabilities, α^i , and ionization energies, I_p^i ,^{26,27} leading to 63.16 for Pb and 0.7 for O Jnm⁶mol⁻¹, respectively. The C_6^i for heavy elements (*e.g.* Sn, Pb) were simply extrapolated from those of lighter elements of the same group,^{26,27} resulting in rather approximated values. Furthermore, the electronic nature (covalence or ionicity) of atomic species vary depending on the local chemical environment, imposing some limitations in the use of the atomic-like parameters. In order to give a better estimation of the C_6^i values one should find a way to account for the different

chemical environments of a given atomic species. Different methods to re-parametrize the C_6^i for ionic systems have been proposed,^{46,47} but, the C_6^i values were derived *ad hoc* for each system, reducing their transferability. In this study we derive the C_6^i parameters for each ionic species in a *ab initio* fashion following as close as possible the protocol suggested by Grimme by enforcing the role of the specific environment for each atomic species (details in the supplementary material). On elementary considerations, the net charges of the Pb and O ions should be +2 and -2, respectively. Mulliken analysis, albeit quite dependent on the adopted basis set, gives a much reduced values of +1 and -1, respectively. Nevertheless, Löwdin charges calculated using a PP-PW approach agree with the Mulliken's picture. Using a pragmatic approach we compute the ionization potential and polarizability for the bare Pb^+ and Pb^{2+} ions using a Stuttgart ECP with a QVZ basis set. The same methodology cannot be adopted for computing these quantities for O^- and O^{2-} , since both species are unstable with respect to the free atom. In the latter case we have adopted a method proposed for MgO by Tosoni and Sauer⁴⁸ to set up a proper environment for oxygen in order to get both O^- and O^{2-} as stable species. As described in the supplementary information we average the values of the polarizabilities over the two Pb^+/Pb^{2+} and O^-/O^{2-} states to account for the semi-ionic nature of the PbO oxides. Since the ionization potentials are intrinsically discontinuous variables we choose to adopt the values for the Pb^{2+} and O^{2-} to be used in the definition of the dispersion coefficient C_6^i . Within this assumption the final C_6^i , with Eq. (3b), for Pb and O, become 36.93 and 0.54 Jnm mol⁻¹, respectively (see supplementary Information). The new C_6^i are smaller than the atomic-like ones reported by Grimme. The geometrical mean of the single C_6^i parameters (see Eq. (3a)) results in a mean C_6 (PbO) equal to 4.48 Jnm mol⁻¹, which is found smaller than that proposed by Grimme, *i.e.* 6.64 Jnm mol⁻¹, avoiding the occurrence of spurious over-binding effects. In summary two flavors of DFT-D2 were employed: *i*) using the Grimme's parameters (PBE-D2) and *ii*) using the recalculated C_6^i (PBE-DC2) according to the scheme presented here. Results are shown in Table 1.

4 Results and discussion

Results are outlined through three thematic sections: in Section 4.1 we address the description of the geometrical properties of the PbO phases, while discussing the effect of dispersion on these materials. This section terminates with an insightful investigation of the lone-pairs nature using the electric field gradient. Section 4.2 discuss the elastic properties, while Section 4.3 vibrational frequencies.

4.1 Geometry

Both α and β -PbO polymorphs crystallize in a layered arrangement.^{12,13,16–18,49} The PbO layered stacking and the interlayer distances ($l-l$, see Figure 1), are controlled by lone-pairs on the Pb-sites. The resulting deformed electron cloud (of Pb^{2+}) produces an electric dipole that along with dispersion forces collectively drive the layers to stack. Structures, of Table 1, were obtained after full structural relaxation (at 0 K) from experimental X-ray data of the PbO phases.^{50,51}

Table 1 shows how the LCAO method reproduces with good accuracy both the experimental^{50,51} and previous LDA-DFT data.^{12,13,16–18,49} With PBE we found the α phase more stable than β one consistently with experimental evidences ($\Delta E = 3.22 \text{ kJ mol}^{-1}$ per formula unit⁻¹). **On the other hand the distorted α phase, observed at low temperature, is negligibly more stable (at the PBE level) than the α one for about $0.040 \text{ kJ mol}^{-1}$ per formula unit.**

Among the GGA functionals PBE is by far more accurate than BLYP; the latter largely overestimates the $l-l$ distance together with the lattice parameters a and c . Eventually B3LYP and PBE0, further increase the magnitude of the lattice parameters (see Table 1). α -PbO turns into β -PbO at 4.15 GPa with PBE (2.80 GPa with LDA), while experimental data ranges from 3 up to 3.6 GPa.⁵² From this preliminary evaluation PBE appears to be the best choice and therefore it will be used to discuss the dispersion effects throughout the paper. Non-surprisingly functionals based on Becke exchange (BLYP and B3LYP) show an over-repulsive behavior compared to Perdew's functionals (PBE, PBE0) in agreement to Ref. 53.

Table 1: lattice parameters a , b and c (in Å), c/a ratio, Volume (in Å³) and interlayer $l-l$ distance (see Fig Figure 1, in Å) of α , β -PbO. Data in bracket are BSSE corrected.

α -PbO $P4/nmm$	a	c	V	c/a	$l-l$
Exp. ^a	3.975	5.023	39.7	1.263	2.6
PBE ^b	4.097	5.096 (5.600)	41.9	1.221(1.367)	3.0
PBE-PW ^c	3.985	5.579	45.8	1.400	3.2
PBE-D2 ^b	4.049	4.584 (4.766)	37.6	1.132 (1.180)	2.4
PBE-D2-PW ^c	3.985	4.762	37.8	1.195	2.4
PBE-DC2 ^b	4.066	4.648 (4.848)	38.4	1.143 (1.192)	2.5
PBE-DC2-PW ^c	3.980	4.835	38.9	1.215	2.5
PBEsol ^b	4.035	4.690	38.2	1.162	2.3
PBE0 ^b	4.021	4.996	40.4	1.242	2.6
BLYP ^b	4.144	5.746	49.3	1.386	3.3
B3LYP ^b	4.073	5.691	47.2	1.397	3.3
LDA-PZ ^d	3.956	4.874	38.1	1.232	–
LDA-PZ ^e	3.953	4.988	–	–	–
LDA-PZ ^f	3.910	4.930	–	–	–
β -PbO $Pbcm$	a	b	c	V	$l-l$
Exp. ^g	5.893	5.490	4.753	153.8	3.2
PBE ^b	6.213	5.587	4.823	167.4	3.5
PBE-PW ^c	6.293	5.805	4.800	147.9	3.6
PBE-D2 ^b	5.499	5.324	4.732	145.3	2.8
PBE-D2-PW ^c	5.541	5.388	4.846	144.7	2.8
PBE-DC2 ^b	5.688	5.413	4.836	148.9	2.9
PBE-DC2-PW ^c	5.636	5.445	4.836	148.4	2.9
PBEsol ^b	5.962	5.302	4.762	150.5	3.2
PBE0 ^b	6.174	5.586	4.704	162.2	3.4
BLYP ^b	6.554	5.868	4.879	187.7	3.8
B3LYP ^b	6.471	5.798	4.791	179.8	3.7
LDA-PZ ^f	5.770	5.380	4.680	–	–

^aRef.⁵⁰ X-Ray; ^bThis work, LCAO; ^cThis work, PP-PW; ^dRef.^{12,13} PP-PW; ^eRef.¹⁸ PP-PW; ^fRef.¹⁶ augmented spherical-waves; ^gRef.⁵¹ X-Ray.

4.1.1 The effect of the dispersion

While dispersion is accounted for both phases, the detailed discussion only concerns α -PbO. Insights on the layered structure of PbO is given by ΔE_{ly} , which determines the extent of the interaction between two PbO sub-layers:

$$\Delta E_{ly} = E_c - E_\infty \quad (4)$$

where E_c is the energy of two PbO layers, with atoms in the same geometrical relationships as in the bulk structure, at a given inter-layer distance (see $l-l$ in Figure 1) and E_∞ is the energy of two PbO layers well separated and non-interacting. ΔE_{ly} is the energy cost of extracting a PbO sheet from the bulk (see Figure 1). Practically, this is done by running several SCF points at increasing lattice parameters (*i.e.* c for α -PbO), eventually affecting the $l-l$ distance between 2 PbO layers. The real effect of the dispersion contribution, introduced by DFT-D2 or DFT-DC2, should only affect the ΔE_{ly} magnitude. Figure 2 shows the behavior of ΔE_{ly} at increasing lattice parameters c in α -PbO.

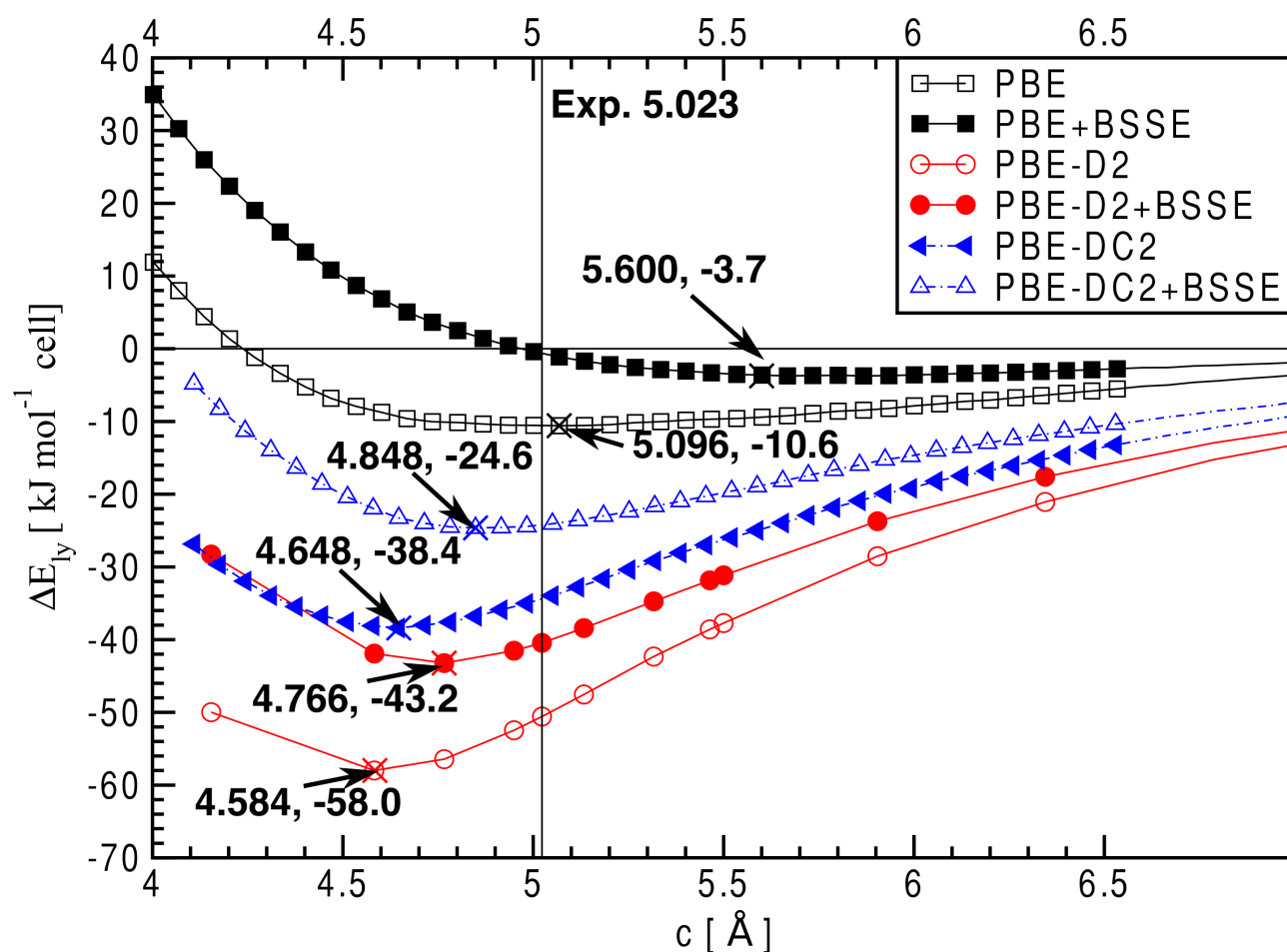


Figure 2: ΔE_{ly} , and ΔE_{ly}^C vs. c for α -PbO using the PBE, PBE-D2 and PBE-DC2. ΔE_{ly} in kJ mol⁻¹ and c in Å. The current graph is shortened at 7 Å, but SCF calculations were run up to 40 Å (c) where ΔE_{ly} is null.

In Figure 2, ΔE_{ly} changes dramatically when the D correction is introduced (see both PBE–D2 and PBE–DC2 cases). The PBE curve presents a very shallow minimum of $-10.6 \text{ kJ mol}^{-1}$. The correction introduced on E_{ly} by PBE–D2, $-58.0 \text{ kJ mol}^{-1}$, is of 47.4 kJ mol^{-1} with respect to plain PBE. The PBE–DC2 data lies between the PBE and the PBE–D2 curves ($-38.4 \text{ kJ mol}^{-1}$, see Figure 2). The empirical dispersion term, E_D of Eq. (1) and Eq. (2), to the total energy promotes the inter-layer interaction forcing a decrease in the interlayer spacing. In α -PbO the reduction of the c lattice constant is the clear evidence of an increase in the layer-layer interaction. The final magnitude relies totally on the size of the C_6^i parameters that enters Eq. (2). The large binding contribution of PBE–D2 and the PBE–DC2, is affected by the BSSE. The BSSE has a two-fold effect: *i*) it reduces the relative ΔE_{ly} (*i.e.* shifting the binding-curve to more negative ΔE_{ly} values over-binding PbO layers), *ii*) artificially reduces the magnitude of c . The BSSE was calculated using the counterpoise correction, and was practically done by introducing ghost functions on the two PbO layers while they were progressively separated. Knowing the magnitude of the BSSE one can re-calculate the corrected dispersion curve, whose minimum results shifted from the non-corrected one. The PBE BSSE corrected c value is 5.600 \AA , which is largely overestimated with respect to the experimental value (see Table 1, data in parentheses). Calculations with the PBE functional using *PWscf* (BSSE free) confirmed our findings with the LCAO method. Summarizing, the PBE functional largely overestimates the lattice parameters involved in the stacking process. All LCAO data of Table 1 when corrected for BSSE are shifted to larger values. PBE–D2 over-binds the α -PbO structure ($c = 4.584 \text{ \AA}$, see Table 1), whereas when corrected for the BSSE, the c value (4.766 \AA) moves towards the experimental value (5.023 \AA) but still underestimated. This is confirmed by the PP–PW calculations. On the other hands the re-parametrization of Grimme’s coefficients introduces a visible improvement in the geometry description of α -PbO. The c value (after correcting for the BSSE) is found in good agreement with the experimental value (4.848 \AA). This also agrees with PP–PW calculations ($c = 4.835 \text{ \AA}$). With PBE–DC2 α -PbO is more stable than the β phase by 3.6 kJ mol^{-1} per formula unit and also comparable with the PBE value 3.2 kJ mol^{-1} per formula unit. This shows that dispersion is very similar for the two PbO phases.

Although we did not calculate the ΔE_{ly} for the β polymorph a very similar behavior of Figure 2 is expected. In the next sections only data obtained with PBE and PBE-DC2 will be considered, disregarding the PBE-D2.

Although the reproduction of band-gap is not appropriate with DFT, the introduction of the dispersion reduces the band-gap simply through the decrease of the the c parameter, which for α -PbO is 2.9 eV with PBE and it becomes 2.8 eV PBE-DC2 and 2.2 eV with PBE-D2. As observed by Allen *et al.*⁴⁷ the band-gap decrease is concomitant with the reduction of the c parameter. This is the only effect noticeable by looking at the band structure and density of state plots (not reported here).

4.1.2 Electric field gradient and quadrupole coupling constants

The electric field gradient tensor (EFG) is beneficial to understand how the PbO lone-pairs arrange within the interlayer space (see distance $l-l$ in Figure 1).⁵⁴ EFG components: V_{11} , V_{22} and V_{33} are ordered according to their magnitudes $V_{11} \leq V_{22} < V_{33}$. Relevant is the EFG asymmetry, η , calculated as $\eta = \frac{|V_{22}| - |V_{11}|}{|V_{33}|}$, whereas the quadrupole coupling constant (QCC) is computed from V_{33} :

$$QCC = \frac{e^2 q_m Q}{h} = \frac{e Q V_{33}}{h} \quad (5)$$

with e the electron charge and Q the atomic quadrupole moment. EFG tensor components, η , and QCC values for ^{17}O and ^{204}Pb are shown in Table 2 and Figure 3.

V_{33} in α -PbO confirms that the lone-pair is oriented along the c axis as previously observed with electron localization functions (ELF) plots.¹⁸ The lone-pair of Pb atoms in the β -phase is found at an angle of 125.9, 38.2 and 101.5 degrees with respect to lattice constants a , b and c , respectively. Differently from the α -phase in β -PbO the Pb lone-pairs are not entirely oriented in one direction and similar evidences were discussed by Rault *et al.*¹⁸ Friedemann *et al.*⁵⁵ affirmed that the QCC for the β -polymorph (158.96 MHz) is larger than the corresponding QCC (96.82 MHz) value in the α -phase, which agrees with our results. Our *ab initio* data is also confirmed by

Table 2: PBE EFG components, η and QCC for the following nuclei: ^{17}O and ^{204}Pb of α and β -PbO. Z for nucleus. V_{xx} are expressed in 10^{-1} e a.u. $^{-3}$ (1 e a.u. $^{-3} = 9.717 \times 10^{21}$ Vm $^{-2}$), QCC in MHz.

Z	V_{11}	V_{22}	V_{33}	QCC	η
α -PbO $P4/nmm$					
Pb ^a	-5.00	-5.00	10.00	104.17	0.00
O ^b	-1.88	-1.88	3.76	1.13	0.00
β -PbO $Pbcm$					
Pb ^a	-3.16	-9.32	12.50	130.21	0.16
O ^b	-0.49	1.14	2.14	1.64	0.06

^aRef. ⁵⁵ experimental $Q(^{204}\text{Pb}) = 4.42 \times 10^{-29}$ m 2 ; ^bRef. ⁵⁶ experimental $Q(^{17}\text{O}) = -2.56 \times 10^{-30}$ m 2 .

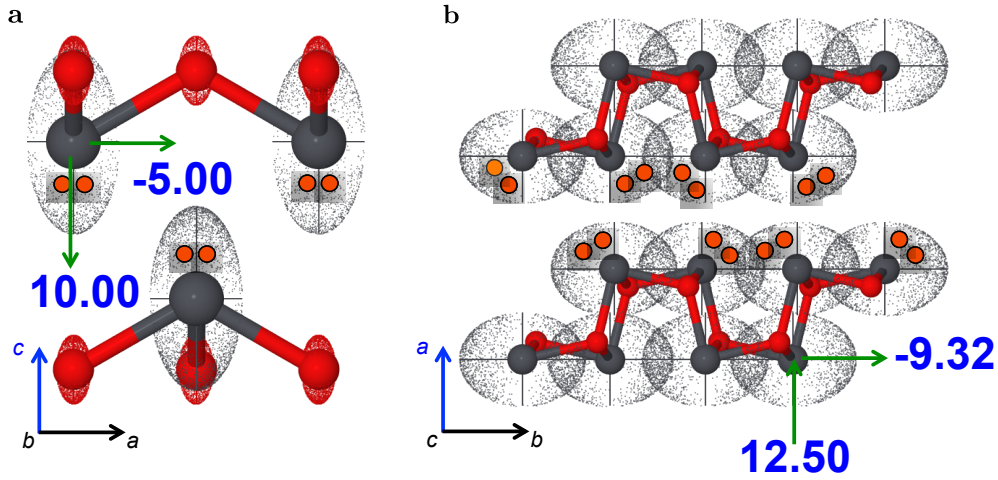


Figure 3: EFG principal components (arrows) superimposed on the two PbO structures, a) α , b) β , respectively. V_{11} , V_{22} and V_{33} refers to data in Table 2 and are in 10^{-1} e a.u. $^{-3}$. Orange circles represent the lone-pairs within the interlayer zone.

LAPW simulations (β -QCC 151.55 α -QCC 93.55 MHz, respectively).⁵⁵ Le Bellac *et al.*⁵⁷ also observed that the phase transition $\alpha \rightarrow \beta$ is accompanied by an evident change in orientation of the lone-pair. PBE-DC2 EFG components are equal to those calculated with plain PBE showing that dispersion interactions are too weak to alter the component of the electron density at nuclei.

4.2 Elastic properties

Table 3 shows the elastic constants and bulk moduli of α and β -PbO calculated with the PBE and PBE-DC2 functionals.

Table 3: PBE, PBE–DC2 elastic constants C_{ij} and bulk moduli B (calculated *via* elastic constants), in GPa, for α and β -Pb. DC2 refers to PBE–DC2.

	C_{11}	C_{22}	C_{33}	C_{44}	C_{55}	C_{66}	C_{12}	C_{13}	C_{23}	B
α -PbO $P4/nmm$										
PBE ^a	64.7	64.7	16.3	10.9	10.9	54.4	64.6	14.7	14.7	36.9
PBE–DC2 ^a	53.2	53.2	30.2	18.7	18.7	44.2	51.3	20.0	20.0	35.5
LDA ^b	–	–	–	–	–	–	–	–	–	24.0
Exp. ^c	–	–	–	–	–	–	–	–	–	23.1
β -PbO $Pbcm$										
PBE ^a	42.1	45.5	96.6	39.8	7.8	1.8	6.9	11.9	27.0	30.6
PBE–DC2 ^a	48.4	47.3	102.2	30.6	22.5	2.9	7.2	12.8	25.4	32.1
LDA ^d	–	–	–	–	–	–	–	–	–	31.1

^aThis work, LCAO; ^bRef. ^{12,13} PP–PW; ^cRef. ⁵² Exp.; ^dRef. ¹⁷ PP–PW.

Bulk moduli of Table 3 are very similar to previous LDA simulations and experimental value in the case of α -PbO, ^{12,13,17,52} confirming the soft nature of these materials. Previous LDA simulations ^{12,13} behave slightly better than our PBE results. Bulk moduli for the β -phase are in closer agreement with the experimental data. Although the calculated elastic constants are consistent with the geometries of the PbO-phases, the experimental values are currently not available. For α -PbO C_{11} , C_{22} (64.7 GPa) are larger than C_{33} (16.3 GPa) suggesting that the distortion along the [001] direction is easier (see Table 3), which agrees with the layered-structure. The inverse trend is obtained for α -PbO shear stresses. The effect exerted by the lone-pair on β -PbO is smaller than in the α -phase; in fact C_{11} (42.1 GPa) acting orthogonally to the [100] direction (*i.e.* the a direction) is similar to C_{22} (45.5 GPa), which acts along the zig-zag chains. The strain along the C_{33} (96.6 GPa) remains the hardest one according to the structural arrangement. Mixed strains (C_{12} , C_{13} , and C_{23}) and pure shear stresses (C_{44} , C_{55} and C_{66}) are consistent with the geometry definition of both lead oxide-phases. We observed that PbO macroscopic densities increase when the α phase is irreversibly transformed into its β one. Bulk moduli and elastic constants calculated with PBE–DC2 are similar to PBE. **PBE–DC2 improves the bulk modulus of α PbO toward the experimental value.**

4.3 Phonon frequencies at the Γ point

Γ point phonon frequencies were computed by using PBE and PBE–DC2. The relevant infrared (IR), Raman frequency window for both monoxides, is relatively narrow: 100–500 cm^{-1} .⁵⁸ This is likely to cause overlapping between near bands as confirmed by Adams *et al.*⁵⁸ α –PbO, with space group $P4/nmm$ (D_{4h}^7) gives rise to 9 vibrational modes (see Eq. (6)). The PbO– β phase $Pbcm$ (D_{2h}^{11}) shows 21 vibrational modes (see Eq. (6)).

$$\begin{aligned}\Gamma^\alpha &= A_{1g} + A_{2g} + B_{1g} + B_{2g} + 2E_g + \\ &+ A_{1u} + A_{2u} + B_{2u} + 2E_u\end{aligned}\quad (6a)$$

$$\begin{aligned}\Gamma^\beta &= 3B_{2u} + 4B_{1g} + 4A_g + 2B_{2g} \\ &+ 3B_{3u} + 2A_u + B_{1u} + 2B_{3g}\end{aligned}\quad (6b)$$

Vibrational frequencies calculated within the LCAO approximation are intrinsically affected by the BSSE error. To understand the magnitude of the BSSE on the final result we have compared the IR/Raman frequencies computed with Gaussian basis–set calculations with those obtained with a PP–PW approach (*i.e.* $PWscf$). Results reported in the supplementary material show a good agreement between the two dataset implying that BSSE does not dramatically affect the vibrational frequencies.

4.3.1 α –PbO

Of the nine modes of α –PbO two are IR active (A_{2u} and E_u); while Raman spectrum consists of four modes (A_{1g} , B_{1g} and $2E_g$). E modes degenerate showing same atomic displacements, but orthogonal one another. Table 4 compares the calculated IR and Raman frequencies with the experimental data and their graphical representation is shown in Figure 4.

Raman modes A_{1g} and B_{1g} involve only the motion of lead and oxygen atoms parallel to the c axis, while the A_{2u} mode is an anti–phase motion of Pb and O atoms. E_u and $2E_g$ show atomic

Table 4: IR, Raman (R) frequencies, in cm^{-1} , of α -PbO. Simulated intensities are only available for IR modes (in km mol^{-1}). A. for activity, Irep. for irreducible representation, Int. for intensity, E for experimental. Experimental IR and Raman frequencies were measured by Adams *et al.*,⁵⁸ while theoretical data is only available for IR.⁴⁹ Whenever the experimental data is available $\Delta\nu$ is calculated from this value.

Irep.	A.	ν					$\Delta\nu$		IR Int.	
		PBE	PBE-DC2	LDA ^a	E IR ^b	E R ^b	PBE	PBE-DC2	PBE	PBE-DC2
E_g	R	405	413	–	–	321	84	92	–	–
A_{2u}	IR	387	366	399	470	–	-83	-104	655	810
B_{1g}	R	332	340	–	–	338	-6	2	–	–
E_u	IR	230	264	275	243	–	-13	21	2269	2789
A_{1g}	R	149	154	–	–	146	3	8	–	–
E_g	R	79	101	–	–	81	2	22	–	–

^aRef.⁴⁹ PP-PW; ^bRef.⁵⁸ single crystal specimen at 295 K.

displacements in the ab planes. Possible overlapping between IR and Raman bands is well documented in the previous literature.^{58,59} For example in the α -PbO IR spectrum, mode A_{2u} falls over the E_u one forming a broad band around 290⁵⁹ and 278 cm^{-1} .⁵⁸ Reflectance IR spectroscopy⁵⁸ successfully resolved the single bands in two distinct peaks:¹ *i.e.* 470 cm^{-1} (A_{2u}) and 243 cm^{-1} (E_u , see Table 4). A rather large discrepancy is seen for the PBE A_{2u} mode (-83 cm^{-1}), which gets even worse with PBE-DC2 (-104 cm^{-1}). For the E_u mode a much better agreement is seen with some influence of dispersion. In general, the inclusion of dispersive interactions via PBE-DC2 does not introduces substantial changes to the IR and Raman modes. As noticed by Ugliengo *et al.*,⁶⁰ there is no direct dispersion correction to the vibrational frequencies as they only change due to a different optimum geometry. Theoretical LDA IR frequencies (see Table 4),⁴⁹ agree with our PBE and PBE-DC2 data. Degeneracy occurring for E_u modes make them more intense than the A_{2u} peak as demonstrated by PBE and PBE-DC2 IR intensities. PBE and PBE-DC2 Raman frequencies are in much better agreement with experimental data than the IR ones. This excludes the E_g mode, which suffers a large ipso-chromic shift inverting the experimental order $B_{1g} > E_g$. However, the experimental intensity of this mode is very weak.⁵⁸

¹Here, only transversal modes are discussed.

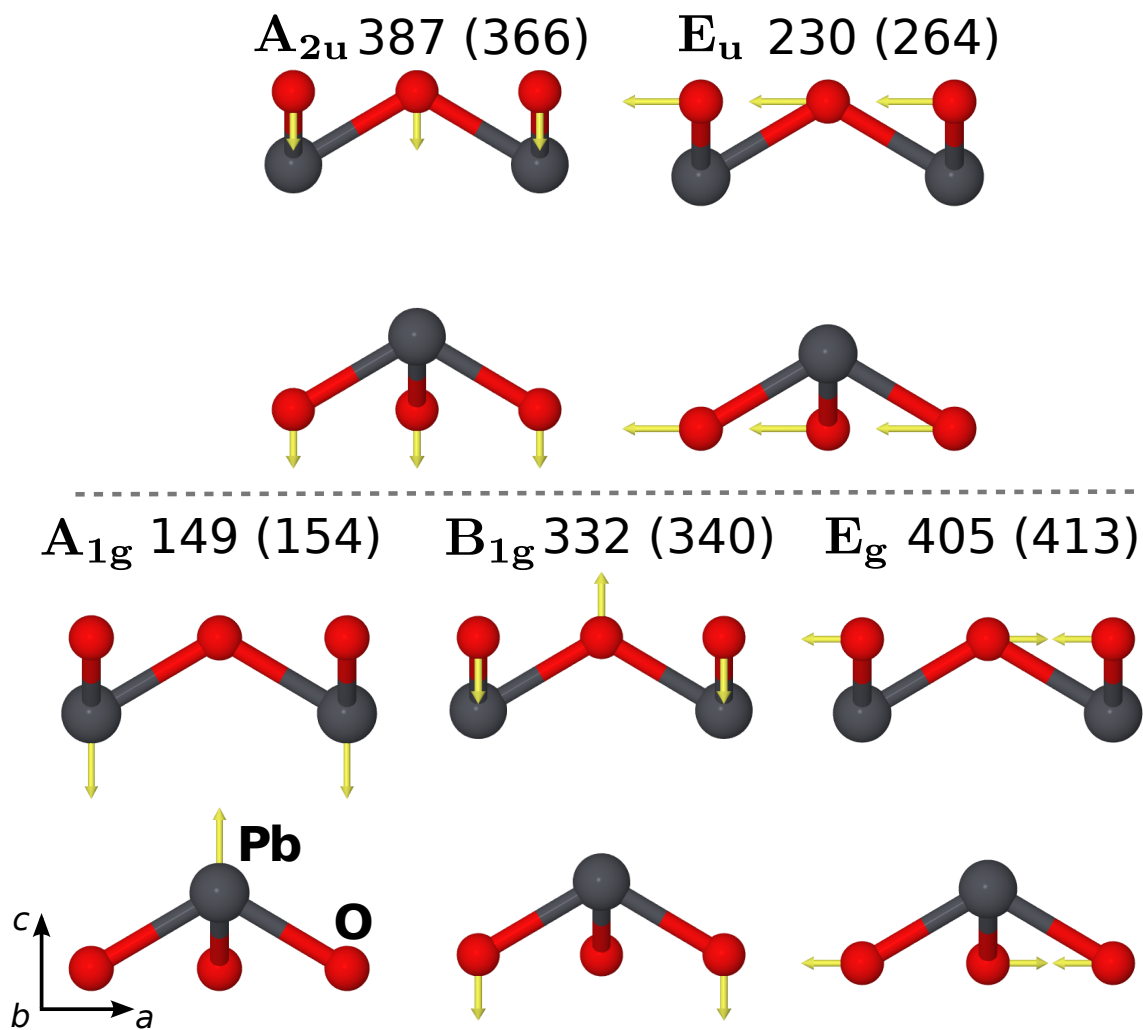


Figure 4: active IR (on the top part) and Raman (on the bottom part) modes for α -PbO in cm^{-1} . Only one degeneracy is shown for vibrational modes classified as E . PBE-DC2 values in brackets

4.3.2 β -PbO

For β -PbO IR active modes are all those *ungerade* (anti-phase deformation) such as $3B_{2u}$, $3B_{3u}$ and B_{1u} , whereas the Raman activities are all *gerade* (in phase deformation) $4B_{1g}$, $2B_{2g}$, $2B_{3g}$ and $4A_g$. $2A_u$ modes are neither IR nor Raman active, hence they will be not discussed. In Figure 5 are only shown the graphical atomic displacements of certain modes, which fall at “high-frequencies” ($500\text{--}200\text{ cm}^{-1}$, exception is B_{1u}) i.e. B_{2u} , B_{3u} for IR, B_{1g} , A_g , B_{2g} and A_u for Raman modes.

An electric vector along b stimulates the B_{2u} modes, whereas a vector along c the B_{1u} ; both

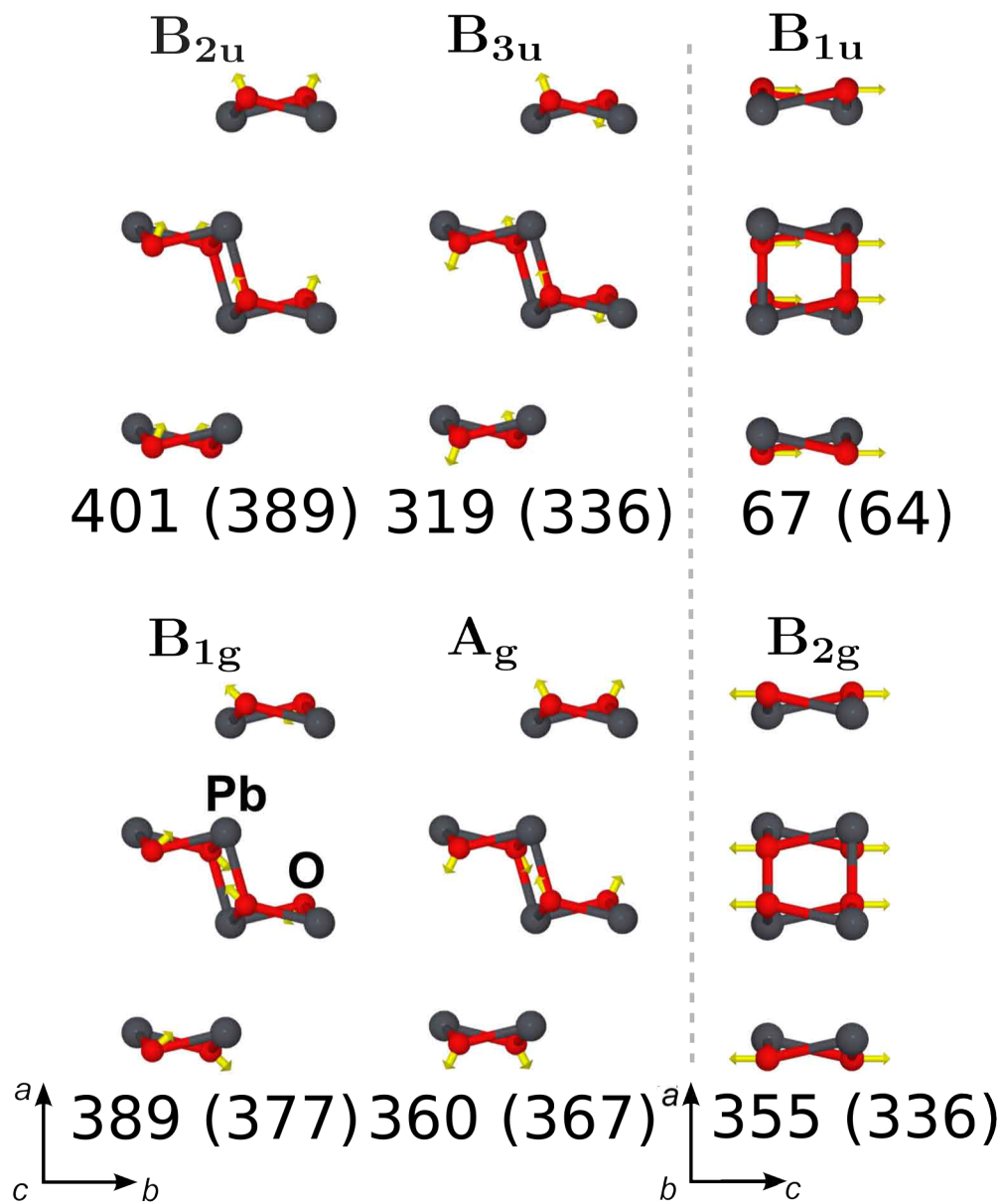


Figure 5: Selection of active IR (on the top part) and Raman (on the bottom part) modes for β -PbO in cm^{-1} . Dash line separates modes with different cell-orientation. PBE-DC2 values in brackets.

vectors laid normal to the planes formed by the sandwiched arrangement of β -PbO (see Figure 5 and Figure 1b). Table 5 compares the present results with previous experimental works the IR (along with its simulated intensities), Raman frequencies.

Adams *et al.*,⁵⁸ assigned the main bands to their respective vibrational modes. Simulated fre-

Table 5: IR, Raman (R) frequencies, in cm^{-1} , of α -PbO. Simulated intensities are only available for IR modes and expressed in km mol^{-1} . A. stands for activity, *i* for inactive, Irep. for irreducible representation, Int. for intensity, E is for experimental. Experimental IR and Raman frequencies values were measured by Adams *et al.*,⁵⁸ while theoretical values are only available for IR.⁴⁹ Whenever the experimental data is available $\Delta\nu$ is calculated from this value.

Irep.	A	ν					$\Delta\nu$		IR Int.	
		PBE	PBE-DC2	LDA ^a	E IR ^b	E R ^b	PBE	PBE-DC2	PBE	PBE-DC2
B_{2u}	IR	401	389	418	356	–	45	33	1391	1913
B_{1g}	R	389	377	–	–	385	4	8	–	–
A_g	R	360	367	–	–	349	11	18	–	–
B_{2g}	R	355	336	–	–	–	–	–	–	–
B_{2u}	IR	350	337	281/360	290	–	60	45	65	168
B_{3u}	IR	319	336	281/360	424/500	–	-181	-165	816	795
B_{1g}	R	310	313	–	250	–	60	63	–	–
A_u	<i>i</i>	293	272	–	–	–	–	–	–	–
A_g	R	279	270	–	289	–	-10	-19	–	–
B_{3u}	IR	266	270	281/360	424	–	-158	-154	1219	1538
B_{3g}	R	222	235	–	171	–	51	64	–	–
B_{2u}	IR	122	136	–	146	–	-24	-10	0	0
A_g	R	90	100	–	87	–	3	13	–	–
B_{2g}	R	86	111	–	72	–	14	39	–	–
B_{1g}	R	68	74	–	52	–	16	22	–	–
B_{1u}	IR	67	64	78	–	–	-11	-14	2947	3321
A_u	<i>i</i>	65	83	–	–	–	–	–	–	–
B_{3u}	IR	59	64	–	–	–	–	–	14	21
B_{3g}	R	56	76	–	–	–	–	–	–	–

^aRef. ⁴⁹ PP-PW; ^bRef. ⁵⁸ single crystal specimen at 295 K.

quencies below 68 cm^{-1} are reported in Table 5, however they were not revealed experimentally. PBE and PBE-DC2 IR frequencies are similar to both experimental⁵⁸ and previous theoretical ones.⁴⁹ This is particularly true for the B_{2u} mode that suffers a small ipso-chromic shift from the experimental value. Waghmare *et al.* found the same trend using a PP-PW approach.⁴⁹ Puzzling is the comparison of the B_{3u} modes, which seems underestimated by PBE by 181 cm^{-1} . This mode involves the motion of both Pb and O right across the layered structure (see Figure 5). The PBE-DC2 slightly improve this mode. The correct assignment of the B_{3u} modes is also not very clear from the experimental point of view, since other modes such A_g and B_{3g} would overlap and mix with this modes. Adams *et al.* claimed that these bands could be assigned to overtones.⁵⁸ Waghmare and co-workers addressed this issue reporting a possible spectral window $281\text{--}360\text{ cm}^{-1}$,⁴⁹ underestimating the experimental values. Raman frequencies agree very well with those assigned experimentally. The B_{1g} mode suffers of a small up-shift. The other modes fell below this threshold, concluding that our simulation describe the Raman spectrum with good accuracy.

5 Conclusion

We demonstrated the use of LCAO approach within the DFT framework to address different properties of lead monoxide polymorphs. We tested several GGA and hybrid functionals, in order, to predict as good as possible the PbO geometrical properties. Among the adopted functionals PBE is the best option as Becke’s exchange based functionals (BLYP and B3LYP) largely overestimated the cell parameters. The correct geometry is, however, only reproduced when the dispersion interaction is included. In that respect, a new strategy to re-parametrize Grimme’s coefficients for Pb and O in PbO is presented, which can be extended also to other semi-ionic solids. **This is based on the use of *ab initio* polarizabilities and ionization potentials, which account for the crystalline environments experienced by the ions.** The introduction of dispersive interactions was found essential to reproduce the experimental cell parameters for both PbO polymorphs and shown to be the major component of the inter-layer interaction. In accordance with previous computational works our

data justify different anisotropy of the Pb lone-pair within the two lead monoxide polymorphs, and this is further confirmed by the quadrupolar coupling constants. Elastic constants clearly show how the α -phase is affected by a larger anisotropy than β one, which eventually reflects the lone-pair orientation within the two PbO-phases. The PBE PbO phonons, at the Γ -point, for both phases are only in moderate agreement with the experiment and inclusion of dispersion at PBE-DC2 slightly worsen the agreement for the alpha-phase while it remains almost the same for the beta one. As anharmonicity should not play a key role for these systems we suspect that the Grimme's approach to account for dispersion does not improve frequencies as it has only an indirect effect through the change in the equilibrium geometry. Further study is needed to clarify this matter.

Acknowledgement

This research was supported by a UKC Scholarship from University of Kent. The authors would like to acknowledge the use of the UK National Grid Service in carrying out this work. PC and PU are very thankful to Dr. Marta Corno and Dr. Bartolomeo Civalleri of the Department of Chemistry, University of Torino. We are finally very thankful to both referee for their profound and insightful comments.

References

- (1) Pan, Z. W.; Dai, Z. R.; Wang, Z. L. *Appl. Phys. Lett.* **2002**, *80*, 309.
- (2) Sun, P.; Matsuura, N.; Ruda, H. F. *J. Appl. Phys.* **2004**, *96*, 3417 – 3423.
- (3) Murphy, J. E.; Beard, M. C.; Norman, A. G.; Ahrenkiel, S. P.; Johnson, J. C.; Yu, P. R.; Micic, O. I.; Ellingson, R. J.; Nozik, A. J. *J. Am. Chem. Soc.* **2006**, *128*, 3241–3247.
- (4) Takaishi, T.; Jin, J.; Uchino, T.; Yoko, T. *J. Am. Chem. Soc.* **2000**, *83*, 2543.
- (5) Fujino, S.; Hwang, C. S.; Morinaga, K. *J. Am. Chem. Soc.* **2004**, *87*, 10–16.

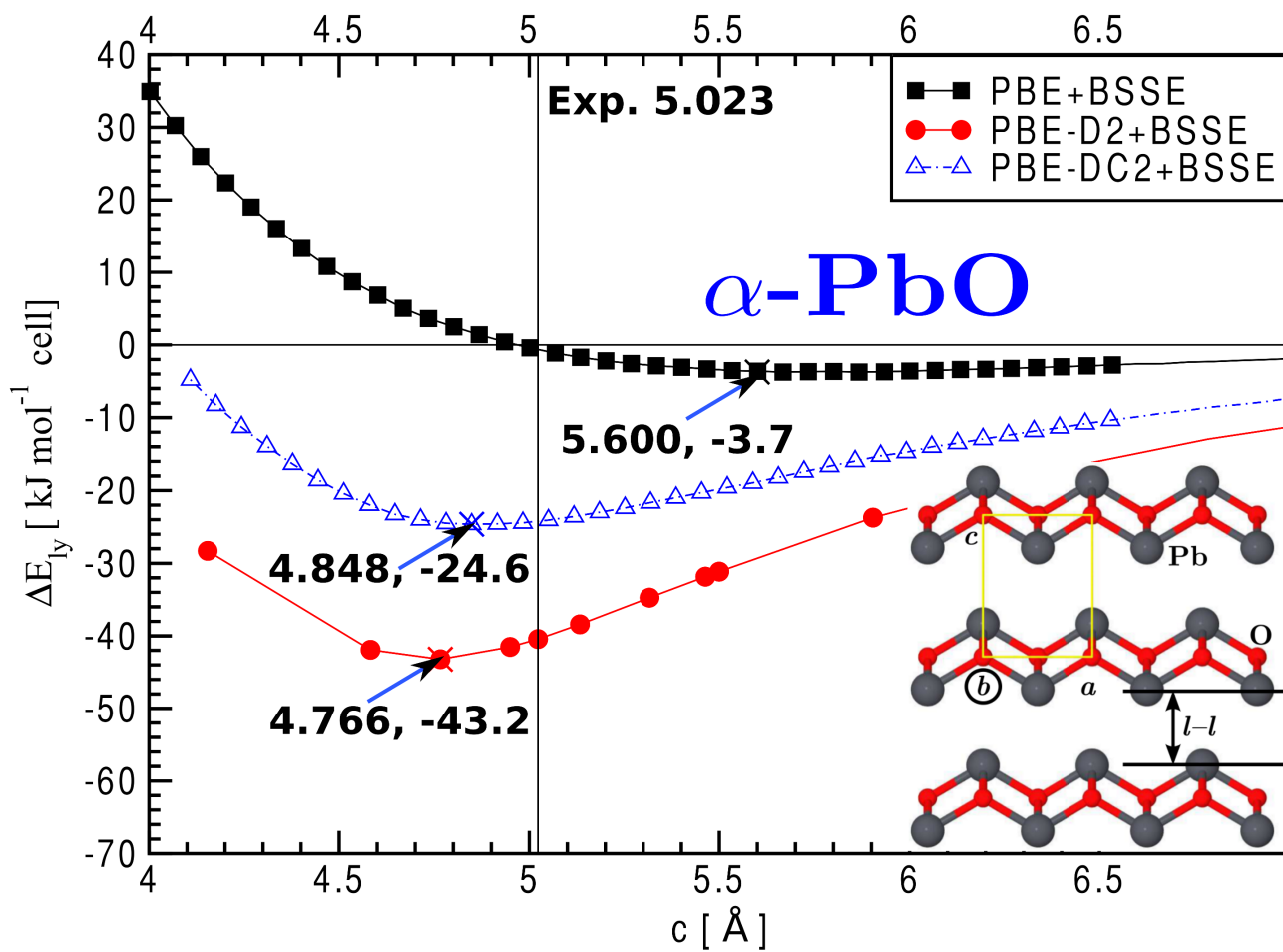


Figure 6: TOC

- (6) McCann, L. I.; Trentelman, K.; Possley, T.; Golding, B. *J. Raman Spectrosc.* **1999**, *30*, 121–132.
- (7) Pilania, G.; Tan, D. Q.; Cao, Y.; Venkataramani, V. S.; Chen, Q.; Ramprasad, R. *J. Mater. Sci.* **2009**, *44*, 5249 – 5255.
- (8) Heideman, G.; Noordermeer, J. W. M.; Datta, R. N. *Kautsch. Gummi Kunstst.* **2005**, *58*, 30–42.
- (9) Nanda, M.; Tripathy, D. K. *Polym. Polym. Comps.* **2010**, *18*, 417–427.
- (10) Cruz, M.; Hern?n, L.; Morales, J.; S?nchez, L. *J. Power Sources* **2002**, *108*, 35–40.
- (11) Ahuja, R.; Blomqvist, A.; Larsson, P.; Pyykkö, P.; Zaleski-Ejgierd, P. *Phys. Rev. Lett.* **2011**, *106*, 018301.
- (12) Watson, G. W.; Parker, S. C. *J. Phys. Chem. B* **1999**, *103*, 1258–1262.
- (13) Watson, G. W.; Parker, S. C.; Kresse, G. *Phys. Rev. B* **1999**, *59*, 8481–8486.
- (14) Boher, P.; Garnier, P.; Gavarrı, J. R.; Hewat, A. W. *J. Sol. State Chem.* **1985**, *57*, 343–350.
- (15) Evarestov, R. A.; Veryazov, V. A. *Phys. Status Solidi B* **1991**, *165*, 401–410.
- (16) Terpstra, H. J.; de Groot, R. A.; Haas, C. *Phys. Rev. B* **1995**, *52*, 11690–11697.
- (17) Haussermann, U.; Berastegui, P.; S., C.; Haines, J.; Ledger, J.-M. *Angew. Chem. Int. Ed.* **2001**, *40*, 4624–4628.
- (18) Raulot, J.-M.; Baldinozzi, G.; Seshadri, R.; Cortona, P. *Solid State Sci.* **2002**, *4*, 467–474.
- (19) French, R. H. et al. *Rev. Mod. Phys.* **2010**, *82*, 1887–1944.
- (20) Dion, M.; Rydberg, H.; Schröder, E.; Langreth, D. C.; Lundqvist, B. I. *Phys. Rev. Lett.* **2004**, *92*, 246401.

- (21) Thonhauser, T.; Cooper, V. R.; Li, S.; Puzder, A.; Hyldgaard, P.; Langreth, D. C. *Phys. Rev. B* **2007**, *76*, 125112.
- (22) Lee, K.; Murray, E. D.; Kong, L.; Lundqvist, B. I.; Langreth, D. C. *Phys. Rev. B* **2010**, *82*, 081101.
- (23) Vydrov, O. A.; Van Voorhis, T. *Phys. Rev. Lett.* **2009**, *103*, 063004.
- (24) Zhao, Y.; Schultz, N. E.; Truhlar, D. G. *J. Chem. Phys.* **2005**, *123*, 161103.
- (25) Zhao, Y.; Truhlar, D. G. *Acc. Chem. Res.* **2008**, *41*, 157–167.
- (26) Grimme, S. *J. Comput. Chem.* **2004**, *25*, 1463.
- (27) Grimme, S. *J. Comp. Chem.* **2006**, *27*, 1787.
- (28) Grimme, S.; Antony, J.; Ehrlich, S.; Krieg, H. *J. Chem. Phys.* **2010**, *132*, 154104.
- (29) Tkatchenko, A.; Scheffler, M. *Phys. Rev. Lett.* **2009**, *102*, 073005.
- (30) Tkatchenko, A.; Robert A. DiStasio, J.; Head-Gordon, M.; Scheffler, M. *J. Chem. Phys.* **2009**, *131*, 094106.
- (31) Dovesi, R.; Civalleri, B.; Orlando, R.; Roetti, C.; Saunders, V. R. *Reviews in Computational Chemistry*; John Wiley & Sons, Inc, New York, 2005; Vol. 21; Chapter 1, pp 1–126.
- (32) Dovesi, R.; Saunders, V. R.; Roetti, C.; Orlando, R.; Zicovich-Wilson, C. M.; Pascale, F.; Civalleri, B.; Doll, K.; Harrison, N. M.; Bush, I. J.; D’Arco, P.; Llunell, M. *CRYSTAL09, User Manual*. 2009.
- (33) Perdew, J. P.; Burke, B.; Ernzerhof, M. *Phys. Rev. Lett.* **1996**, *77*, 3865–3868.
- (34) Perdew, J. P.; Ruzsinszky, A.; Csonka, G. I.; Vydrov, O. A.; Scuseria, G. E.; Constantin, L. A.; Zhou, X.; Burke, K. *Phys. Rev. Lett.* **2008**, *100*, 136406.
- (35) Becke, A. *Phys. Rev. A* **1988**, *38*, 3098 – 3100.

- (36) Lee, C.; Yang, W.; Parr, R. G. *Phys. Rev. B* **1988**, *37*, 785 – 789.
- (37) Becke, A. D. *J. Chem. Phys.* **1993**, *98*, 5648–5652.
- (38) Adamo, C.; Barone, V. *J. Chem. Phys.* **1999**, *110*, 6158–6170.
- (39) Schafer, A.; Horn, H.; Ahlrichs, R. *J. Chem. Phys.* **1992**, *97*, 2571.
- (40) Metz, B.; Stoll, H.; Dolg, M. *J. Chem. Phys.* **2000**, *113*, 2563–7.
- (41) Peterson, K. A.; Figgen, D.; Goll, E.; Stoll, H.; Dolg, M. *J. Chem. Phys.* **2003**, *119*, 11099–11112.
- (42) Monkhorst, H. J.; Pack, J. D. *Phys. Rev. B* **1976**, *13*, 5188 – 5192.
- (43) Perger, W. F.; Criswell, J.; Civalleri, B.; Dovesi, R. *Comput. Phys. Commun.* **2009**, *180*, 1753–1759.
- (44) Pascale, F.; Zicovich-Wilson, C. M.; López Gejo, F.; Civalleri, B.; Orlando, R.; Dovesi, R. *J. Comp. Chem.* **2004**, *25*, 888–897.
- (45) Giannozzi, P. et al. *J. Phys.-Condens. Mat.* **2009**, *21*, 395502.
- (46) Conesa, J. C. *J. Phys. Chem. C* **2010**, *114*, 22718–22726.
- (47) Allen, J. P.; Scantlon, D. O.; Parker, S. C.; Watson, G. W. *J. Phys. Chem. C* **2011**, *115*, 19916–19924.
- (48) Tosoni, S.; Sauer, J. *Phys. Chem. Chem. Phys.* **2010**, *42*, 14330–40.
- (49) Waghmare, U.; Rabe, K. In *Materials Fundamentals of Gate Dielectrics*; Demkov, A. A., Navrotsky, A., Eds.; Springer Netherlands, 2005; pp 215–247.
- (50) Wyckoff, R. W. G. *Crystal structure I*; Interscience Pub., 1963; pp 85–237.
- (51) Hill, R. J. *Acta Crystallogr. C* **1985**, *41*, 1281–1284.

- (52) Giefers, H.; Porsch, F. *Physica B* **2007**, *400*, 53–58.
- (53) Wu, X.; Vargas, M. C.; Nayak, S.; Lotrich, V.; Scoles, G. *J. Chem. Phys.* **2001**, *115*, 8748.
- (54) Kaufmann, E. N.; Vianden, R. *J. Rev. Mod. Phys.* **1979**, *51*, 161–214.
- (55) Friedemann, S.; Heinrich, F.; Haas, H.; Trüger, W. *The Nuclear Quadrupole Interaction of ^{204m}Pb in Lead Oxides*; Springer Netherlands, 2004; Vol. 159; pp 313–322.
- (56) Pyykkö, P. *Z. Naturforsch.* **1992**, *47a*, 189–196.
- (57) Le Bellac, D.; Kiat, J.-M.; Hedoux, A.; Garnier, P.; Grebille, D.; Guinet, Y.; Noiret, I. *Ferroelectrics* **1992**, *125*, 215–220.
- (58) Adams, D.; Stevens, D. *Dalton Trans.* **1976**, *371*, 1096–1103.
- (59) Donaldson, J.; Donoghue, M.; Ross, S. D. *Spectrochim. Acta. A* **1974**, *30*, 1967–1975.
- (60) Ugliengo, P.; Zicovich-Wilson, C. M.; Tosoni, S.; Civalieri, B. *J. Mater. Chem.* **2009**, *19*, 2564–2572.